Radial-radial correlation and energy transfer in higher doubly excited $^1S^e$ helium states by partial-wave analysis

Bao Cheng-guang
Department of Physics, Zhongshan University, Guangzhou, People's Republic of China
(Received 26 January 1989; revised manuscript received 10 April 1989)

The $N=3$ series of the $^1S^e$ helium states have been investigated by partial-wave analysis and by observing the shape densities. The K-classification scheme has been recovered. The strong radial-radial correlation region (SRRCR) has been found. The process of energy transfer occurring inside the SRRCR has been inspected in detail and two types of mechanisms, the "direct push" and the "head-on collision," have been discovered.

I. INTRODUCTION

The investigation of electron-electron (e-e) correlation has had a long history, and many physicists have been attracted to this important topic. In the case of the two-electron system, the classification scheme of the excited states has been worked out,[1] and the distribution of the electrons in hyperspherical coordinates[2] and in the body frame,[3,4] has been extensively explored, in particular, in the $N\leq 2$ series. Nevertheless, not much work has been done on the higher excited series ($N\geq 3$); thus they deserve to be systematically investigated in detail.

This paper is a continuation of two previous papers, Refs. 4 and 5. The same procedure as in Ref. 4 is used to diagonalize the Hamiltonian to obtain the eigensolutions of the $^1S^e$ helium states. However, we are now interested in the $N=3$ series which are scarcely concerned in Ref. 4. For this purpose we enlarge and adjust the basis functions to include more $N=3$ components in our model space (248 basis functions are chosen in the model space originally; however, after dropping nearly dependent components, the model space is 145-dimensional). In fact, it is difficult to obtain very accurate solutions of highly excited states. Neither the solutions obtained in Ref. 4 nor the solutions obtained in this paper are accurate enough for quantitative purpose. Nonetheless, the present work will improve the accuracy a little if only $N=3$ series are concerned. As before, the aim of this paper is to obtain qualitative features of the electron-electron (e-e) correlation by making systematic analysis of the wave functions. Since the angular correlation of the electrons originates from the interference of different partial waves, in order to have a deeper understanding of the e-e correlation it is necessary to have a complete understanding of the partial-wave structure. Hence we shall decompose a given eigensolution Ψ as

$$\begin{aligned}\Psi&=\sum_l |(ll)_0\rangle\langle(ll)_0|\Psi\rangle \\ &=\sum_l |(ll)_0\rangle\frac{(-1)^l F^{(l)}(r_1,r_2)}{r_1 r_2}\ , \\ |(ll)_0\rangle&=\frac{(-1)^l\sqrt{2l+1}}{4\pi}P_l(\cos\theta)\ .\end{aligned} \tag{1}$$

Here Ψ is considered as a function of $\mathbf{r}_1$ and $\mathbf{r}_2$ which are the position vectors of the electrons originating from the nucleus, l is the angular momentum of an electron relative to the nucleus, and θ is the angle between $\mathbf{r}_1$ and $\mathbf{r}_2$. $F^{(l)}(r_1,r_2)$ is the partial-wave radial function which will be analyzed in detail in the following.

From $F^{(l)}$ we define the weight of a given partial wave of a given state as

$$B^{(l)}=\int dr_1\, dr_2 |F^{(l)}(r_1,r_2)|^2 \tag{2}$$

fulfilling

$$\sum_l B^{(l)}=1\ . \tag{3}$$

This quantity reveals the relative importance of different partial waves. The third quantity we shall investigate is the shape density $\rho_s(r_1,r_2,\theta)$ defined in Ref. 4 which is the probability density of a given state of the system staying at a given shape and a given orientation (zero total angular momentum states are isotropic). This quantity is introduced to expose the geometric aspect of the system. The shape where the shape density arrives at its maximum $\rho_s^{\max}$ is the most probable shape. This shape is labeled by $(\bar{r}_1,\bar{r}_2,\bar{\theta})$ fulfilling

$$\rho_s(\bar{r}_1,\bar{r}_2,\bar{\theta})=\rho_s^{\max}\ . \tag{4}$$

The results are presented as follows.

II. RESULTS AND DISCUSSION

The calculated eigenenergies are given in the third column of Table I. They are, in general, close to the results by Lipsky, Anania, and Conneely[6] listed in the fourth column. The m and K numbers of the ${}_m(K,T)^A_N$ classification scheme[1,2] are listed in the first and the second column, respectively. In the states concerned in this paper, they have $T=0$, $A=+$, and $N=3$, thus they may be simply labeled as (m,K). In the following, m labels the mth state of a subseries having a given K.

From Table I we found that the energy of the $(m,-2)$ state is extremely close to the $(m+2,2)$ state. This feature implies that there is something unusual in the $K=-2$ states and will be discussed later.

The $B^{(l)}$ are given in Table II, parts (a), (b), and (c) for $K=2$, 0, and -2 states, respectively. From Table II, part (a) we found that the $K=2$ states are dominated by a mixture of S and P waves; when m gets larger, B^S gets smaller, B^P and B^D get a little larger. From Table II, part (b) we found that the S and D waves are more important than the P wave in the $K=0$ states: when m gets larger, B^S gets larger, B^P and B^D get a little smaller. From Table II, part (c) we found that the $K=-2$ states are dominated by a mixture of P and D waves; besides, though the F wave is considerably weaker than the S wave it is no longer negligible.

Since parts (a)–(c) of Table II show explicitly that states having the same K have similar composition of partial waves, it is expected that they would have similar features in structure. We have justified this suggestion by systematically observing the eigensolutions. We will not present all the results but only those of some specific states to avoid tediousness. In each case the behavior of the electrons will be viewed from partial-wave analysis and from a geometric aspect as follows.

TABLE I. Eigenenergies of the $N=3$ series of the ${}^1S^e$ helium states to be compared with those by Lipsky. The states are classified by the ${}_m(K,T)^A_N$ scheme and the m and K numbers are given in the first and second column, respectively.

		${}^1S^e$ states ($N=3$ series)	
		E (eV)	
m	K	This work	Ref. 6
1	2	−9.673	−9.638
1	0	−8.654	−8.593
2	2	−7.595	−7.652
2	0	−7.199	−7.161
1	−2	−6.990	−7.004
3	2	−6.950	−6.969
3	0	−6.735	−6.711
2	−2	−6.643	−6.652
4	2	−6.627	−6.639
4	0	−6.507	−6.493
3	−2	−6.455	−6.463
5	2	−6.449	−6.459
5	0	−6.376	−6.369
4	−2	−6.342	−6.351
6	2	−6.335	
6	0	−6.265	

TABLE II. The weights $B^{(l)}$ of the $K=2$, 0, and -2 states are given in parts (a)–(c), respectively, to show the composition of the partial waves in these three types of states.

m	B^S	B^P	B^D	B^F
		(a) $K=2$		
1	0.55	0.42	0.03	
2	0.53	0.43	0.04	
3	0.50	0.44	0.06	
4	0.48	0.45	0.06	
5	0.47	0.46	0.07	
		(b) $K=0$		
1	0.33	0.23	0.44	0.01
2	0.34	0.20	0.46	
3	0.39	0.20	0.41	
4	0.41	0.20	0.40	
5	0.42	0.19	0.39	
		(c) $K=-2$		
1	0.11	0.32	0.51	0.06
2	0.11	0.34	0.53	0.02
3	0.11	0.35	0.53	0.01
4	0.11	0.36	0.53	0.01

III. $K=2$ SUBSERIES

The $m=3$ state [${}_3(2,0)^+_3$ state] is chosen as a representative. In order to understand the e-e correlation dynamically, we fix r_2 at a number of values; in each case $F^{(l)}$ as functions of r_1 are given as a set of curves in a figure. Evidently this set of curves describes the behavior of e_1 when r_2 is prescribed. Observing how this set of curves varies with r_2, we can understand how the motion of e_1 responds to the motion of e_2. Four figures with r_2 fixed at 13.31, 6.0, 4.5, and 3.2 Å are chosen to be shown in Figs. 1(a)–1(d), respectively.

In Fig. 1(a) e_2 is far away and is staying inside the outermost peak of the one-body density. In this case e_1 has no chance to go out; thus the curves describe the behavior of the inner electron. We found the following.

(i) The locations of nodes are very close to those of a $Z=2$ Coulomb field, thus each partial wave of the inner electron is simply determined by the nucleus (however, this statement has to be changed if e_2 comes in).

(ii) The existence of e_2 (though it is now far away) causes a very strong mixing of partial waves. In particular, the state is now dominated by the interference of $3S$ and $3P$ waves in reverse phase. The geometric consequence of this interference [simply a cancellation of $P_1(\cos\theta)$ with $P_0(\cos\theta)$] is shown by ρ_s plotted in Fig. 2(a), where we found that the e-e angular correlation is remarkably strong to keep the electrons at opposite sides with $\bar{\theta}=145°$. This is a distinguished geometric character for all positive-K states (though the magnitude of $\bar{\theta}$ may be slightly different). This point was stated in Refs. 2 and 3; we have now confirmed it from the view of interference of partial waves and from an intuitive picture provided by ρ_s.

(iii) Since the inner electron mostly hides itself behind the nucleus, the e-e repulsion is weaker resulting in a

better binding. Hence the energy of the $(m,K=2)$ state is always lower than that of the $(m,K=0$ or $-2)$ state.

(iv) When r_2 varies in a broad region around 13.31 Å, the pattern of Fig. 1(a) does not change, the domain of r_1 in Fig. 1(a) can be roughly divided into two regions. There is no node in region I; accordingly the relative composition (of partial waves) changes slightly with r_1, resulting in a weak radial-angular correlation. On the other hand, three nodes are concentrated in region II; accordingly the relative composition changes strongly with r_1, resulting in a strong radial-angular correlation. Thus region II is a strong radial-angular correlation region (SRACR) defined in Refs. 4 and 5 (in Ref. 4 this SRACR was considered as two separate SRACR's). The probability of the inner electron staying in region II is not very small. Since it moves much more quickly than the outer one, it will enter into this SRACR quite often. In each occasion, its angular momentum will undergo a rapid change resulting in moving in a wiggly manner. Since the outer electron must have exactly the same amount of angular momentum as e_1 (but in reverse direction to keep total angular momentum zero), in each occasion it suffers the same rapid change resulting in moving in a slightly wiggly manner.

In Fig. 1(d) e_2 is in the $N=3$ shell, and the outer part of the curves tells us the behavior of the outer electron. We found the following.

(i) The outer electron is dominated by a mixture of $(m+2)S$ and $(m+2)P$ oscillations in reverse phase.

(ii) The outermost peak is an S peak located at 13.9 Å; thus we suggest that the outer electron is moving in a $Z_{\text{eff}}=1.52$ Coulomb field. It implies that the screening effect of the inner electron is rather poor. The reason is explicit; facing the invasion of the outer electron, it prefers to hide itself behind the nucleus.

Now let us see how Fig. 1(a) is gradually changed in Fig. 1(d) in accord with the intrusion of e_2. When e_2 moves in the $N=5$ shell [the domain of the Nth shell can be found in Fig. 1(d)], nothing happens. When e_2 approaches the $N=4$ shell, a complicated process begins. We found creation, annihilation, and shifting of the nodes; accordingly, the curves vary in complicated manner. We will not present the details but point out the main features.

(i) To compare with Fig. 1(a), we found that the phases of all partial waves have been reversed in Fig. 1(b) and the $N=3$ peaks become much more outward and much broader. Besides, e_1 has now a considerable probability of staying outside the $N=3$ shell. These facts surely imply the occurrence of a strong radial-radial correlation in reverse phase (e_1 goes out when e_2 comes in).

(ii) To compare with Fig. 1(b), we found that there are new nodes created in the inner region of Fig. 1(c). These new nodes will move outward in accord with the decrease of r_2. Accordingly, the $N=3$ peaks of Fig. 1(b) become

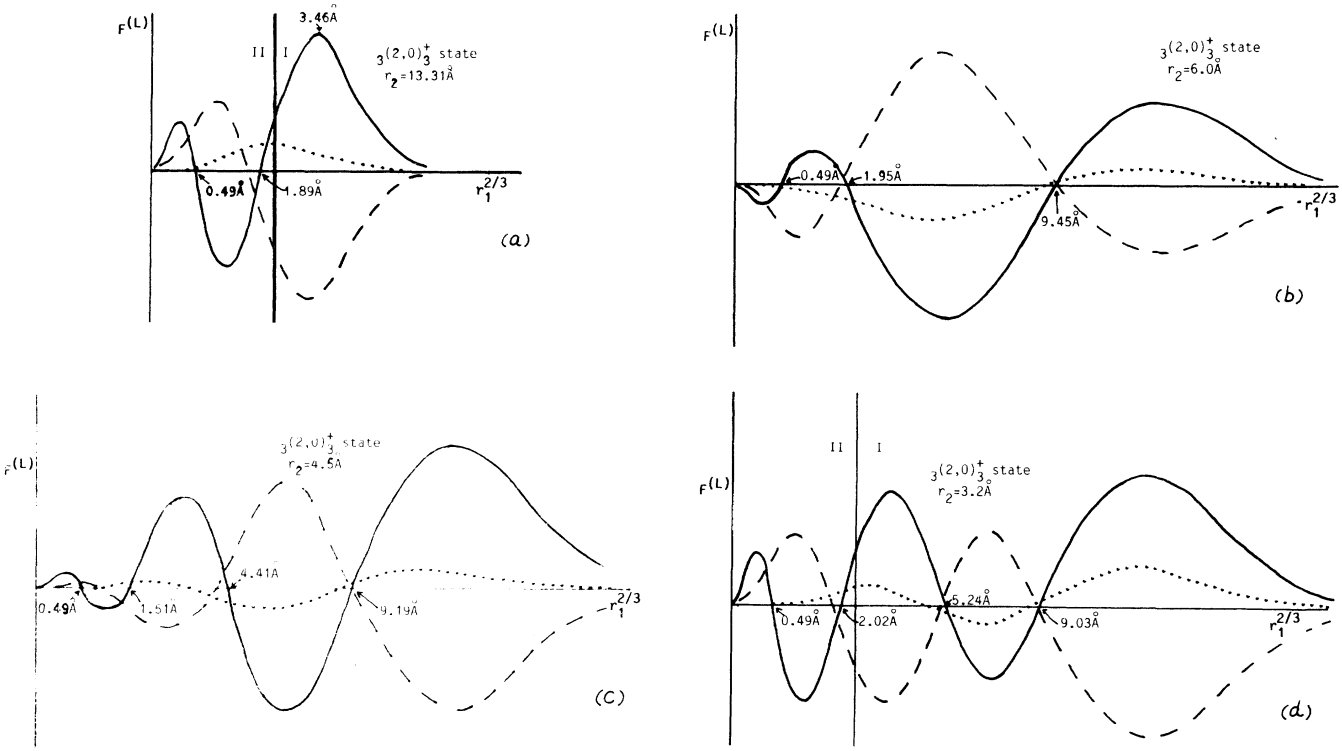

FIG. 1. Partial-wave radial functions $F^{(l)}$ of the $(m=3,K=2)$ state [in ${}_m(K,T=0)^{A=+}_{N=3}$ classification scheme] as functions of r_1 when r_2 is given. In all figures concerning $F^{(l)}$, the S-wave radial function $F^{(l=0)}$ is plotted as a solid line, the P-wave as a dashed line, and the D-wave as a dotted line; all the $F^{(l)}$ are given in arbitrary units and the abscissa is proportional to $r_1^{2/3}$.

the $N=4$ peak in Fig. 1(c). The creation and shift of node implies an accelerating process to speed up the e_1 to go outward. As a result, e_1 has a larger and larger probability of staying outside as shown by the outermost peaks of Fig. 1(c) which are much higher than those in Fig. 1(b).

(iii) An important feature in this process is that the composition of partial waves mainly stays unchanged during the invasion of e_2. The geometric implication is that e_1 remains behind the nucleus. Thus it is pushed outward by e_2 from its back. For this reason we call this a "direct push" mechanism for energy transfer.

Furthermore, since the geometric feature remains unchanged in this process, we can fix θ at $\bar{\theta}$ and observe the shape density ρ_s as a function of r_1 and r_2 to see how they are correlated. A contour diagram is shown in Fig. 3(a) with θ given at 145°. It is clear that there is no correlation in the $N=5$ shell (the small peak in the $N=1$ shell cannot be seen in this figure); however, when e_2 approaches the $N=4$ shell and moves further to the $N=3$ shell, a strong radial-radial correlation takes place. Consequently, e_1 gives up its original way of motion and is gradually pushed from the $N=3$ shell to the $N=4$ shell to eventually form an $N=5$ oscillation. The region where the strong radial-radial correlation occurs is called a strong radial-radial correlation region (SRRCR) marked in the figure.

For other states in this subseries, since they have similar composition, the above qualitative features hold for all of them. In particular, they have the same geometric feature, the same mechanism for energy transfer taking place in the same region. In other words, they have the same diagram as Fig. 3(a) with the same striking SRRCR (but the number of outer peaks may be different). The only exception is the head state [the $m=1$ state, refer to Fig. 3(c) of Ref. 4] where the speedup process characterized by the creation and shift of inner nodes is not found.

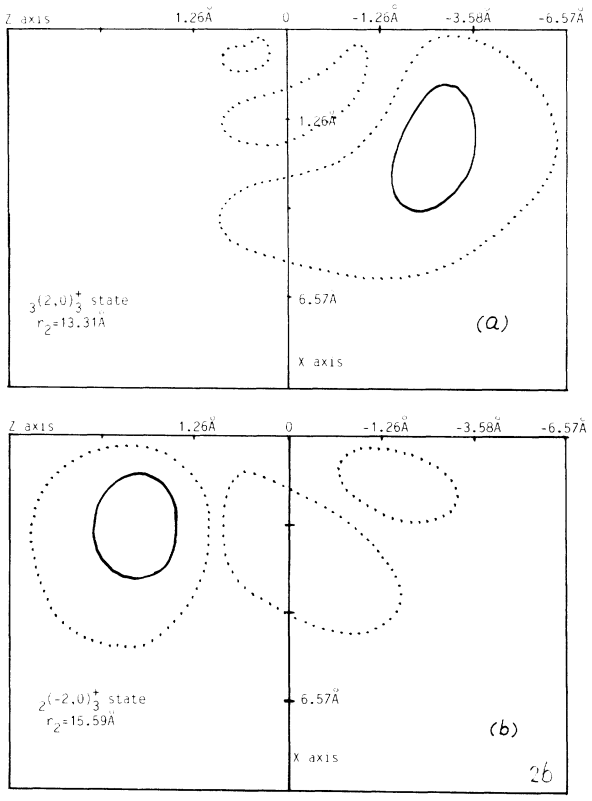

FIG. 2. Shape densities ρ_s of the (3,2) and (2,−2) states are plotted in the X-Z plane as a function of $\mathbf{r}_1$ when e_2 is given at 13.31 and 15.59 Å along the $+Z$ axis, respectively, to show the distribution of the inner electron. In all figures concerning ρ_s, the distance shown in the figure is proportional to $r_1^{2/3}$ (or $r_2^{2/3}$). The contours give $\rho_s=\alpha\rho_s^M$ (where ρ_s^M is the largest value of the shape density in a figure); the dotted line has $\alpha=\frac{1}{20}$, while the solid line has $\alpha=\frac{1}{2}$.

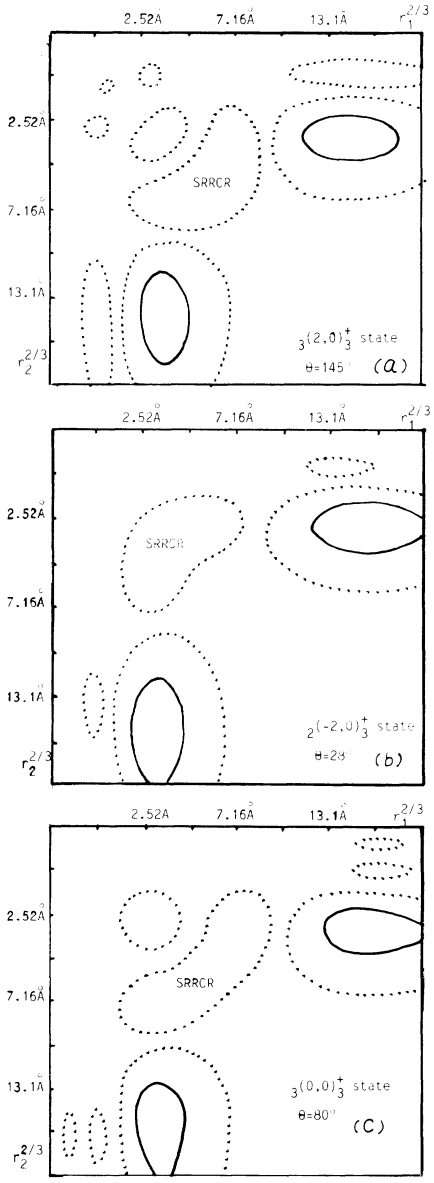

FIG. 3. ρ_s of the (3,2), (2,−2), and (3,0) states are plotted as functions of r_1 and r_2 when θ is prescribed. The dotted line has $\alpha=\frac{1}{40}$, while the solid line has $\alpha=\frac{1}{2}$.

IV. $K=-2$ SUBSERIES

The $m=2$ state [$_2(-2,0)^+_3$ state] is chosen as a representative. $F^{(l)}$ as functions of r_1 when r_2 is given at 15.59, 7.0, 4.3, and 3.2 Å is plotted in Figs. 4(a)–4(d), respectively. We found the following.

(i) When an electron is in the $N=3$ shell while the outer one is far away, the wave function is dominated by the P and D waves with the same phase as shown in Fig. 4(a) and the outer part of Fig. 4(d). Thus the negative-K states have a stronger rotation than the positive-K states. Accordingly, the probability of the inner electron being close to the nucleus is very small.

(ii) The geometric consequence of the interference is shown by the ρ_s plotted in Fig. 2(b), where we found that the e-e correlation is remarkably strong to keep the electrons at the same side with $\bar{\theta}=28°$. This is a distinguished geometric character for all negative-K states and was stated in Ref. 2.

(iii) The geometric configuration now is not favorable to binding because the e-e repulsion is stronger. We found that the energy of the $(m,K=-2)$ state is even close to (but a little lower than) the $(m+2,K=2)$ state.

(iv) the outermost peak in Fig. 4(d) is a D peak located at 16.0 Å, it suggests that the outer electron is moving in a $Z_{\text{eff}}=0.71$ Coulomb field. It implies that the screening effect of the inner electron is superior. The reason is explicit; it prefers to stay in front of the nucleus. Consequently, the negative-K states have a larger size. The size of a $(m,K=-2)$ state is close to a $(m+1,K=0)$ state.

On the other hand, each partial wave of the inner electron is determined by a $Z=2$ Coulomb field as in the previous case.

(v) Observing Figs. 4(a)–4(d), we found the broadened $N=3$ shell continuing to be a very broad shell during the intrusion of e_2. The creation of inner nodes [previously shown in Fig. 1(c)] does not occur; instead, a strong F wave appears inside the broad shell [see Fig. 4(c)]. This point is striking because it is inconceivable for a Coulomb field to have the F wave in the $N=3$ shell; hence the Coulomb field must be seriously disturbed due to the two electrons may be rather close to each other. The appearance of the F wave (maybe together with even higher partial waves; however, the latter are not included in our model space) surely implies a strengthening of rotation. Since both electrons now rotate in the same shell with high rotational velocity in reverse direction, a head-on collision between them is inevitable. Thus underlying the broad $N=3$ peak there is a "head-on collision" mechanism of energy transfer. Consequently, in accord with the decrease of r_2, e_1 has larger and larger probability of going outside and the outermost peaks of this set of figures get higher and higher.

(vi) It seems that the e-e repulsion works more efficiently in the D wave under this mechanism. Thus the D wave may be seriously distorted inside the broadened

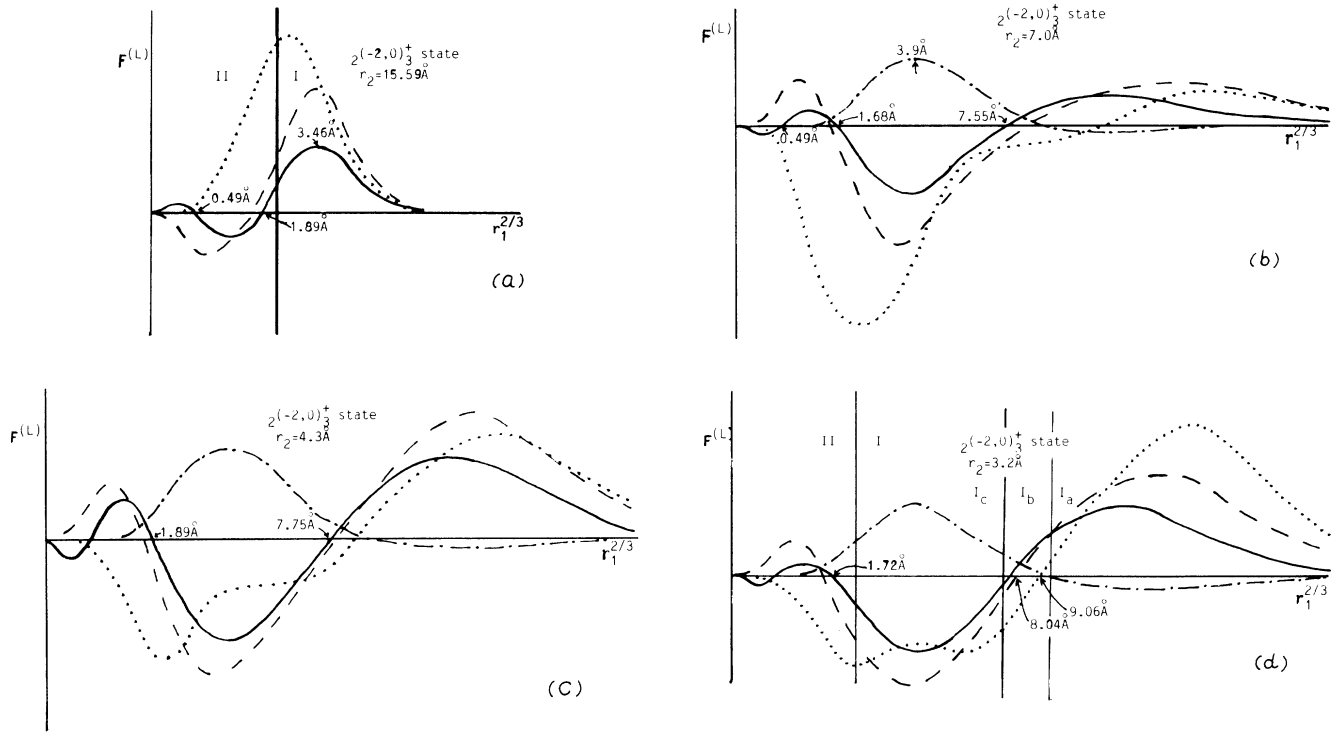

FIG. 4. $F^{(l)}$ of the $(2,-2)$ state are plotted as functions of r_1 when r_2 is given. This set is to be compared with Fig. 1 to show how the behavior of the inner electron is changed when the outer electron comes in. The same notations are used as in Fig. 1; besides, the F wave is depicted in the dash-dotted line. It is evident from (d) that if e_2 stays around 3.2 Å (in the main shell) and if e_1 passes through the narrow region I_b (a SRACR), a strong radial-angular correlation will occur.

shell (where the electrons are, on the average, very close to each other) and the outer D node is pushed remarkably outward. In fact, the outermost node is a D node which overtakes the S and P nodes explicitly.

(vii) During the intrusion of e_2, the D, P, and S waves stay mostly in the same phase. If we omit temporarily the occurrence of the F wave, then the geometric implication is that e_1 stays mostly in front of the nucleus. Thus we can fix $\theta=\bar{\theta}=28°$ and observe ρ_s to see the correlation between r_1 and r_2 as shown in Fig. 3(b) [the small peaks in the $N=1$ shell cannot be seen as in Fig. 3(a)]. It is clear that there is no radial-radial correlation in the $N=4$ shell. When e_2 approaches the $N=3$ shell [the domain of this shell can be found in Fig. 4(d)], the radial-radial correlation occurs, resulting in a broadening of the $N=3$ shell (defined as a SRRCR). Meanwhile, e_1 gives up its original way of motion and rotates more rapidly to suffer a head-on collision with e_2. Afterwards, one of them will go out.

The above qualitative features hold for other states of this subseries. They have the same geometric feature, the same mechanism for energy transfer taking place in the same region. In particular, the broadened $N=3$ shell with remarkable F-wave component is a distinguished common feature of this subseries.

V. $K=0$ SUBSERIES

The $m=3$ state [$_3(0,0)_3^+$ state] is chosen as a representative. $F^{(l)}$ are plotted in Figs. 5(a) and 5(b) where r_2 is given at 15.59 and 3.2 Å, respectively. We found the following.

(i) The S and D waves are a little more important than the P wave while the D wave has opposite phase. The geometric consequence of interference is shown by ρ_s plotted in Fig. 6(a), where the electrons are mostly kept at vertical directions ($\bar{\theta}=80°$). This is a distinguished character of all $K=0$ states as stated in Ref. 2.

(ii) The size of the $(m,K=0)$ state is much smaller than the $(m,K=-2)$ state but is larger than the $(m,K=2)$ state. The outermost peak in Fig. 5(b) is a D peak located at 16.0 Å; it suggests a $Z_{\text{eff}}=1.22$. Thus the screening effect is better than that in the $K=2$ states be-

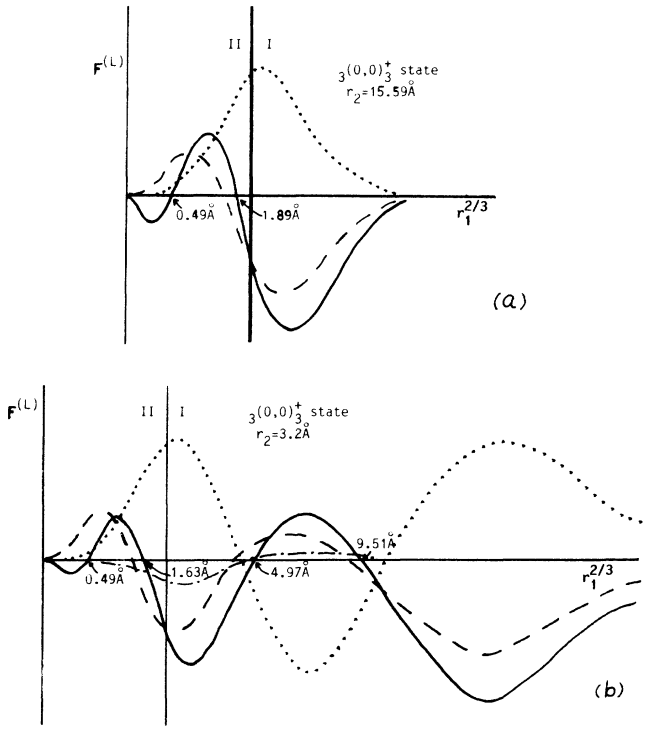

FIG. 5. $F^{(l)}$ of the (3,0) state as functions of r_1 when r_2 is given.

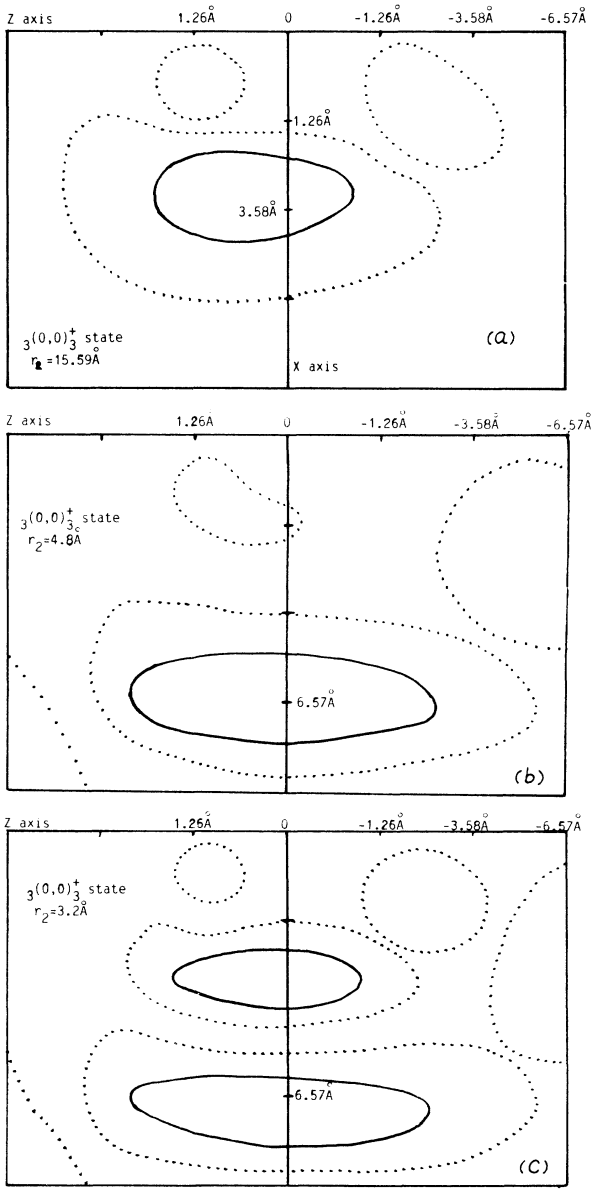

FIG. 6. ρ_s of the (3,0) state plotted in the X-Z plane when $\mathbf{r}_2$ is given at 15.59, 4.8, and 3.2 Å, respectively, along the $+Z$ axis. This set of figures gives an intuitive picture of the "direct push" mechanism for energy transfer.

cause the inner electron is not mostly behind the nucleus now.

In the following, instead of observing the $F^{(l)}$, the process of the intrusion of e_2 is revealed by a set of contour diagrams of ρ_s given in Figs. 6(a)–6(c) with r_2 fixed at 15.59, 4.8, and 3.2 Å, respectively. From this set of figures, not only the "direct push" [shown by the great shift of the great island in Figs. 6(a) and 6(b)], but also the creation of inner nodes [shown in Fig. 6(c)] is explicit. Thus the mechanism of energy transfer is similar to the positive-K states. However, some features belonging to the $K=-2$ subseries, e.g., the appearance of the F wave in the $N=3$ shell, the outer D node overtaking the S and P nodes, may also appear in this subseries to a much weaker extent.

It is noticed that during the invasion of e_2 both electrons are kept at vertical directions. For this reason, we fix θ at $\bar{\theta}=80°$ and observe ρ_s as a function of r_1 and r_2 shown in Fig. 3(c). This figure is similar to Fig. 3(a) but different from 3(b). In particular, the SRRCR extends from the $N=4$ shell to the $N=3$ shell.

Other states of this subseries have the same qualitative feature. However, in the head state ($m=1$) the creation of inner nodes does not occur.

VI. FINAL REMARKS

We have investigated the $N=3$ series of the $^1S^e$ helium states and found the following features.

(i) The K-classification scheme first proposed from group-theory analysis[1] and justified by microscopic calculation[2] has now been further recognized by partial-wave analysis. States belonging to different K subseries have different composition of partial waves, while those belonging to the same subseries have similar composition. As the result of the interference of the partial waves the angular correlation between the electrons is remarkably strong, and each K subseries has its own specific geometric character. This character affects the binding and size of related states.

(ii) From Figs. 2(a), 2(b), and 6(a), we found that the ρ_s is distributed around some ellipselike curve. Although this curve cannot be considered as a trajectory in the classical mechanic sense, it nonetheless reveals the feature of the motion of the inner electron. In Fig. 2(a) ($K=2$), the perihelion of the suggested curve is very close to the center (it implies a small angular momentum) while the aphelion is situated at the opposite side of the outer electron. In Fig. 2(b) ($K=-2$), the perihelion is not so close to the center (it implies a stronger rotation) while the aphelion is situated at the same side with the outer electron. Since the outer electron is rotating (because it is not composed of pure S wave), the distribution of the inner electron as a whole has to rotate synchronously with the outer one to keep the most probable angle $\bar{\theta}$ unchanged.

(iii) Mostly the radial-angular correlation is weak. However, inside the SRACR's the radial-angular correlation is remarkably strong. The origin of SRACR's is the concentration of nodes of different partial waves in some narrower regions.

(iv) The radial-radial correlation is weak outside the SRRCR's; however, it is remarkably strong inside the SRRCR's. In a $K=2$ or 0 state, the SRRCR extends from the $N=3$ shell to the $N=4$ shell; in a $K=-2$ state, it is situated inside the broadened $N=3$ shell.

(v) There are essentially two types of mechanisms for energy transfer. One is a "direct push" existing in the $K=2$ and $K=0$ states; a distinguished feature of this mechanism is the creation and shift of nodes in the inner region. Another one is a "head-on collision" existing in the $K=-2$ states; a distinguished feature of this mechanism is the appearance of higher partial waves inside the SRRCR. Thus the K subseries are also distinguished from each other in the mechanism of energy transfer. It is worth mentioning that two similar mechanisms were found previously by Rehmus and Berry in the atomic autoionization.[7] Now, the mechanisms found in this paper are closely related with the K-classification scheme. It is expected that these mechanisms would be basic and popular in the atomic world.

Although the above qualitative features are extracted from the $N=3$ series, most of them are found to also hold for other series. For example, in the $N=2$ series we found the "direct push" mechanism existing in the $K=1$ (positive) states where the SRRCR extends from the $N=2$ shell (the main shell of this series) to the $N=3$ shell (the outer neighboring shell). Furthermore, we found the "head-on collision" mechanism existing in the $K=-1$ (negative) states where the SRRCR is situated inside the broadened $N=2$ shell [refer to Figs. 6(b) and 6(a) of Ref. 4]. Although we have not investigated the states belonging to the $N\geq 4$ series, it is expected that all the positive-K states have similar geometric features and similar mechanisms for energy transfer. This situation is also expected for all the negative- and zero-K $^1S^e$ helium states. Besides, the existence of the SRRCR is a common characteristic of the spatially symmetric states; however, it does not appear in the spatially antisymmetric states (refer to Fig. 2 of Ref. 5).

We have neglected the relativistic effect. Since this effect is a fine effect, it is expected that this neglect will not spoil the above qualitative results. The method proposed here for analyzing the wave functions is promising for exploring deeper the particle-particle correlation and can also be used for investigating other microscopic systems.

ACKNOWLEDGMENTS

This work is supported by the Natural Science Fund of the Chinese Academy of Sciences.

[1] D. R. Herrick and O. Sinanoglu, Phys. Rev. A **11**, 97 (1975).

[2] C. D. Lin, Phys. Rev. A **12**, 493 (1975); **14**, 30 (1976); **23**, 1585 (1981); **25**, 76 (1982); **25**, 1535 (1982); **29**, 1019 (1984), in *Few-Body Methods: Principles & Applications,* edited by T. K. Lim, C. G. Bao, D. P. Hou, and H.S. Huber (World Scientific, Singapore, 1986), p. 507.

[3] R. Berry, G. S. Ezra, and G. Natanson, in *New Horizons of Quantum Chemistry,* edited by P. O. Löwdin and B. Pullman

(Reidel, Dordrecht, Holland, 1983), p. 77; G. S. Ezra and R. S. Berry, Phys. Rev. A **28**, 1974 (1983); J. E. Hunter III and R. S. Berry, *ibid.* **36**, 3042 (1987).
[4]C. G. Bao, Phys. Rev. A **38**, 591 (1988).
[5]C. G. Bao, Phys. Rev. A **39**, 9 (1989).
[6]L. Lipsky, R. Anania, and M. J. Conneely, At. Data Nucl. Data Tables **20**, 127 (1977).
[7]P. Rehmus and R. S. Berry, Phys. Rev. A **23**, 416 (1981).